Since January 2020 Elsevier has created a COVID-19 resource centre with free information in English and Mandarin on the novel coronavirus COVID-19. The COVID-19 resource centre is hosted on Elsevier Connect, the company's public news and information website.

International Journal of Biological Macromolecules 117 (2018) 704–712

Contents lists available at ScienceDirect

International Journal of Biological Macromolecules

journal homepage: http://www.elsevier.com/locate/ijbiomac

Characterization of the interaction between recombinant porcine aminopeptidase N and spike glycoprotein of porcine epidemic diarrhea virus

Yan-gang Sun [a,b,1], Rui Li [b,1], Longguang Jiang [c,1], Songlin Qiao [b], Yubao Zhi [b], Xin-xin Chen [b], Sha Xie [d], Jiawei Wu [e], Xuewu Li [b], Ruiguang Deng [b], Gaiping Zhang [a,b,d,f,g,*]

[a] College of Veterinary Medicine, Jilin University, Changchun 130062, Jilin, China
[b] Key Laboratory of Animal Immunology of the Ministry of Agriculture, Henan Provincial Key Laboratory of Animal Immunology, Henan Academy of Agricultural Sciences, Zhengzhou 450002, Henan, China
[c] College of Chemistry, Fuzhou University, Fuzhou 350116, Fujian, China
[d] College of Veterinary Medicine, Northwest A&F University, Yangling 712100, Shanxi, China
[e] GE Healthcare Life Sciences, Beijing 100176, China
[f] College of Animal Science and Veterinary Medicine, Henan Agricultural University, Zhengzhou 450002, Henan, China
[g] Jiangsu Co-innovation Center for the Prevention and Control of Important Animal Infectious Diseases and Zoonoses, Yangzhou University, Yangzhou 225009, Jiangsu, China

ARTICLE INFO

Article history:
Received 10 February 2018
Received in revised form 11 May 2018
Accepted 22 May 2018
Available online 24 May 2018

Keywords:
Interaction
Porcine epidemic diarrhea virus
Porcine aminopeptidase N

ABSTRACT

Porcine epidemic diarrhea (PED) has caused huge economic losses to the global pork industry. Infection by its causative agent PED virus (PEDV), an Alpha-coronavirus, was previously proven to be mediated by its spike (S) glycoprotein and a cellular receptor porcine aminopeptidase N (pAPN). Interestingly, some recent studies have indicated that pAPN is not a functional receptor for PEDV. To date, there is a lack of a direct evidence for the interaction between pAPN and PEDV S protein *in vitro*. Here, we prepared pAPN ectodomain and the truncated variants of PEDV S protein in *Drosophila* S2 cells. These recombinant proteins were homogeneous after purification by metal-affinity and size-exclusion chromatography. We then assayed the purified target proteins through immunogenicity tests, PEDV binding interference assays, circular dichroism (CD) measurements, pAPN activity assay and structural determination, demonstrating that they were biologically functional. Finally, we characterized their interactions by gel filtration chromatography, native-polyacrylamide gel electrophoresis (PAGE) and surface plasmon resonance (SPR) analyses. The results showed that their affinities were too low to form complexes, which suggest that pAPN may be controversial as the genuine receptor for PEDV. Therefore, further research needs to be carried out to elucidate the interaction between PEDV and its genuine receptor.

1. Introduction

Coronaviruses are enveloped single-stranded positive-sense RNA viruses, comprising Alpha-, Beta-, Gamma-, and Delta-coronaviruses [1]. They are critical causative agents, whose infections are often associated with respiratory, digestive, and neurological diseases in humans and animals. Among these viruses, two Beta-coronaviruses severe acute respiratory syndrome coronavirus (SARS-CoV) [2–6] and Middle East respiratory syndrome coronavirus (MERS-CoV) [7–10] are lethal to humans, and an Alpha-coronavirus transmissible gastroenteritis virus (TGEV) has caused severe intestinal diseases to pigs [11].

The infection of a coronavirus is mediated by its spike (S) glycoprotein and the S protein is further cleaved into S1 and S2 subunits by endogenous and/or exogenous proteases [12]. The S1 subunit recognizes and binds to the corresponding host receptor, whereas the S2 subunit mediates membrane fusion between the virus and host cells [13–15]. Since intervention of S1 subunit binding to host receptor shows a great antiviral potential, there are increasing studies to elucidate their interaction mechanisms. Angiotensin-converting enzyme 2 (ACE2) [16,17] and dipeptidyl peptidase 4 (DPP4) [18–20] have been identified as the receptor for SARS-CoV and MERS-CoV, respectively. The viral receptor-binding domains (RBD) are located in the C-terminal domains (CTDs) of the S1 subunits (S1-CTDs) [17,19,20]. Human coronavirus 229E (HCoV-229E) [21,22] and TGEV [23,24] utilize aminopeptidase N (APN) as the host receptor and their RBDs are also located in the S1-CTDs [22,24].

Porcine epidemic diarrhea (PED), characterized by vomiting, diarrhea and dehydration, has caused huge economic losses to the global

* Corresponding author at: College of Animal Science and Veterinary Medicine, Henan Agricultural University, Zhengzhou 450002, Henan, China.
E-mail address: zhanggaiping2003@163.com (G. Zhang).
[1] These authors contributed equally to this work.

https://doi.org/10.1016/j.ijbiomac.2018.05.167
0141-8130/

pork industry [25–30]. Its causative agent, PED virus (PEDV), was an Alpha-coronavirus. Previous studies showed that a porcine receptor APN (pAPN) mediated PEDV infection [31–34] and its density appeared to be an important factor in contributing to the virus efficient infection [35]. PEDV S1-CTD (residues 505–629) was further demonstrated to interact with pAPN ectodomain (residues 63–963) [36]. Interestingly, a few recent studies show that pAPN is not the functional receptor for PEDV infection [37,38]. However, there is a lack of direct demonstration of the interaction between pAPN and PEDV S protein to clarify this discrepancy.

In this study, we prepared the extracellular domain of pAPN, PEDV S1 and its truncated variant (S1t) in *Drosophila Schneider* 2 (S2) cells. After purification, we assayed the target proteins for their biological functions. Finally, we characterized their interactions by three canonical assays.

2. Materials and methods

2.1. Cell lines, plasmids, antibodies and reagents

IPEC-J2 cell line (from porcine small intestines) was kindly provided by Zhanyong Wei of Henan Agricultural University, China. Vero cell line (African green monkey kidney epithelial cell line), *Drosophila* S2 cell line, pMT/BiP/V5-His A vector, pCoBlast vector [39,40] and positive serum against PEDV were kept in our laboratory. pEASY-Blunt-pAPN plasmid was constructed and kept in our laboratory. Cellfectin II reagent, blasticidin S, Sf-900 II serum-free medium (SFM) and TRIzol reagent were purchased from Invitrogen (Carlsbad, USA). *Escherichia coli* strain Trans5α competent cells were purchased from TransGen Biotech (Beijng, China). Fetal bovine serum (FBS), Dulbecco's modified Eagle's medium (DMEM), Roswell Park Memorial Institute-1640 medium (RPMI-1640), and antibiotics were purchased from Gibco (Grand Island, USA). Schneider's insect medium, tryptose phosphate broth (TPB), TPCK-trypsin, and L-alanine 4-nitroanilide hydrochloride were purchased from Sigma-Aldrich (St. Louis, USA). The mouse anti-His epitope tag antibody was purchased from Proteintech (Wuhan, China). Horseradish peroxidase (HRP)-conjugated anti-mouse immunoglobulin G (IgG) was purchased from Santa Cruz Biotechnology (Delaware Ave, USA). Pre-stained protein ladder (10 to 180 kDa) was purchased from Thermo Fisher Scientific (Waltham, USA). *Mlu* I, *Bgl* II and Peptide-N-Glycosidase F (PNGase F) enzymes were purchased from New England Biolabs (Massachusetts, USA). Enhanced chemiluminescence (ECL) plus reagent was purchased from Solarbio (Beijing, China).

2.2. Construction of recombinant protein expression vectors

The cDNAs encoding PEDV S1 (residues 21–793) and its truncated variants (residues 21–249, 253–638 and 505–629) were amplified by PCR using the codon-optimized S gene of the PEDV CH/HNXC strain as template. The cDNA encoding pAPN ectodomain (residues 63–963) was amplified by PCR from the pEASY-Blunt-pAPN plasmid. All PCR primers were listed in Table 1. The PCR products were isolated and inserted into the pMT/BiP/V5-His A expression vector between the *Bgl* II and *Mlu* I sites. All constructs were transformed into *Escherichia coli* strain Trans5α competent cells and the recombinant expression vectors were verified by sequencing at Shanghai Sangon Biotech Co. Ltd. (Shanghai, China).

2.3. Cell culture

The *Drosophila* S2 cells were kept in Schneider's insect medium supplemented with 10% heat-inactivated FBS at 28 °C in a humidified incubator. The Vero cells were grown in DMEM supplemented with 10% heat-inactivated FBS at 37 °C in a humidified incubator with 5% CO_2. IPEC-J2 cells were grown in RPMI 1640 medium with 15% heat-inactivated FBS at 37 °C with 5% CO_2. All cell cultures were supplemented with antibiotics (100 U/ml penicillin, 100 μg/ml streptomycin).

Table 1
Primers utilized in this study.

Primer name	Sequence[a]
$S_{21–793}$ F	GGA**AGATCT**CAAGACGTCACCAGGTGCTCG
$S_{21–793}$ R	CG**ACGCGT**GCGGATCGACATCGAGAAGTTG
$S_{21–249}$ F	GGA**AGATCT**CAAGACGTCACCAGGTGCTCG
$S_{21–249}$ R	CG**ACGCGT**ATTGGGCTCAGTGGCAAATACAT
$S_{253–638}$ F	GGA**AGATCT**GGTTTTAGTTTTAATAATTGGTTTC
$S_{253–638}$ R	CG**ACGCGT**GACTCCTACCAGGGGCTTC
$S_{505–629}$ F	GGA**AGATCT**CCATCGTTCAACGATCACAGCT
$S_{505–629}$ R	CG**ACGCGT**GGTGATCAGCTCTCCCTTTGTG
pAPN F	GGA**AGATCT**CAGAGCAAGCCGTGGAACCG
pAPN R	CG**ACGCGT**GCTGTGCTCTATGAACCAATTCAACAC
PEDV qPCR F	CGCAAAGACTGAACCCACTAAC
PEDV qPCR R	TTGCCTCTGTTGTTACTTGGAGAT
PEDV qPCR Probe	FAM-TGTTGCCATTACCACGACTCCTGC-BHQ3

[a] The boldface letters indicate restriction sites.

2.4. Expression of recombinant proteins

The recombinant expression vectors and the pCoBlast vector were co-transfected into *Drosophila* S2 cells by Cellfectin II reagent according to the manufacturer's instructions. The stably transfected S2 cells were selected in Schneider's insect medium supplemented with 10% FBS, antibiotics, and 25 μg/ml blasticidin S. The stably transfected cell lines were then grown in Sf-900 II SFM and induced by 0.75 mM $CuSO_4$ for 5 days. The culture supernatants were harvested by centrifugation at 2000 rpm at 4 °C for 10 min. Expression of recombinant proteins was checked by mouse anti-His epitope tag antibody and HRP-conjugated anti-mouse IgG using Western blot.

2.5. Purification of recombinant proteins

The supernatant containing pAPN ectodomain, PEDV S1 or S1t protein was adjusted to pH 8.0 by 1.5 M Tris-HCl pH 8.8, followed by centrifugation at 10000 rpm at 4 °C for 30 min. After filtration through 0.22 μm filter membranes, the supernatant was applied to HisTrap excel prepacked column (GE Healthcare, Fairfield, USA) or/and HiTrap Q HP prepacked column (GE Healthcare) for purification. Then, each target protein was subjected to size-exclusion column Hiload 16/600 Superdex 200 pg (GE Healthcare) and Superdex 200 increase 10/300 GL (GE Healthcare) for further purification with 20 mM Tris-HCl pH 7.6 and 150 mM NaCl as the elution buffer. The purified proteins were treated with PNGase F according to the manufacturer's instructions. The PNGase F-treated and -untreated proteins were applied to sodium dodecyl sulfate-polyacrylamide gel electrophoresis (SDS-PAGE) under reducing (with β-mercaptoethanol) or non-reducing condition (without β-mercaptoethanol).

2.6. Function analyses of PEDV S1 and S1t proteins

2.6.1. Immunogenicity tests of PEDV S1 and S1t proteins

Purified PEDV S1 and S1t proteins were subjected to SDS-PAGE and transferred to PVDF (polyvinylidene fluoride) membranes. The immunogenicity was then tested by positive serum against PEDV and ECL plus reagent.

2.6.2. PEDV propagation

The PEDV CH/hubei/2016 strain was propagated on Vero cells as previously described [41]. Briefly, when the confluence reached 80%, Vero cells were washed three times and inoculated with 200 $TCID_{50}$ (50% tissue culture infective dose) PEDV at 37 °C for 1 h. After that, the viruses not entering were removed and the cells were cultured with growth medium consisting of 0.3% TPB, 0.02% yeast extract and 3

μg/ml of TPCK-trypsin. When obvious cytopathic effects (CPE) appeared, the cells were frozen and thawed three times, and centrifuged at 2000 rpm at 4 °C for 10 min. Finally, the supernatant was stored at −80 °C for further use.

2.6.3. Interference of PEDV binding by purified S1 and S1t proteins

The IPEC-J2 cells were pre-incubated with indicated concentrations of the purified PEDV S1 or S1t protein for 1 h at 4 °C. Cells were further inoculated with PEDV CH/hubei/2016 strain at an MOI (multiplicity of infection) of 0.1 for 1 h at 4 °C. Then, the virus and protein mixtures were washed away. Total RNA was isolated using TRIzol reagent according to the manufacturer's instructions and the PEDV binding was represented by the copies of the PEDV nucleocapsid (N) gene using absolute quantitative PCR (The primers were listed in Table 1) [42].

2.7. Circular dichroism (CD) measurements of PEDV S1 and S1t proteins

CD measurements (180–260 nm) were carried out on AVIV 420SF spectrometer (Lakewood, USA) at room temperature (RT) using a 1 mm path-length quartz cell. The instrument was calibrated with 10 mM phosphate buffer (PB) pH 7.6, and freshly purified PEDV S1 and S1t proteins were adjusted to 0.8 mg/ml and 1.9 mg/ml in 10 mM PB pH 7.6, respectively. Five scans were accumulated at a scan speed of 1 nm/step with average time of 0.3 s.

2.8. Functional and structural analyses of pAPN ectodomain

2.8.1. Activity assay of pAPN ectodomain

1 nM purified pAPN ectodomain was mixed with 100 μM to 10 mM L-alanine 4-nitroanilide hydrochloride as substrate in 100 μl 60 mM KH_2PO_4 buffer pH 7.2 at 37 °C for 60 min. Then, the product *p*-nitroanilide was measured using a microplate reader (BMG LABTECH, Offenburg, Germany) at 405 nm [43].

2.8.2. Structural determination of pAPN ectodomain

The purified pAPN ectodomain was concentrated to 10 mg/ml in 20 mM Tris-HCl pH 7.2, 150 mM NaCl. Crystallization of pAPN ectodomain was carried out by the sitting-drop vapor diffusion method with an equal volume of the target protein and various crystallization reagents from the crystallization screening kits (Hampton, USA) at RT. The crystals were acquired with a reservoir solution containing 25% (wt/vol) PEG3350, 0.2 M sodium fluoride and 100 mM Hepes pH 7.2. The crystals were flash-frozen in liquid nitrogen using a crystal freezing buffer containing 20% ethylene glycol, 30% PEG3350, 0.2 M sodium fluoride and 100 mM Hepes pH 7.2. X-ray data sets of the crystals were collected at a wavelength of 0.979 Å on the beam line BL19U1 at National Center for Protein Sciences Shanghai (NCPSS) and Shanghai Synchrotron Radiation Facility (SSRF). The crystal structure was solved by molecular replacement [44] using the mammalian APN structure (PDB code: 4HOM) [43] as the search model. The structure was refined by ccp4 program package [44] and manually adjusted by the molecular graphics program COOT [45] until convergence of the refinement. Solvent molecules were added using a Fo-Fc Fourier difference map at 2.5σ in the final refinement step. Statistics of data collection and final model refinement were summarized in Table 2. The coordinates of pAPN ectodomain were deposited in the Protein Data Bank (PDB code 5Z65, http://www.rcsb.org). The final structures were analyzed by software Pymol [46].

Table 2
Kinetics of purified pAPN ectodomain.

pAPN ectodomain	K_m (mM)	K_{cat} (s^{-1})	K_{cat}/K_m ($s^{-1}\cdot mM^{-1}$)
	0.18 ± 0.13	75.55 ± 7.9	420

2.9. Gel filtration chromatography analysis

pAPN ectodomain was mixed with excess PEDV S1 or S1t protein for 1 h at RT in 20 mM Tris-HCl pH 7.6, 150 mM NaCl. Then, PEDV S1 or S1t protein, pAPN ectodomain and their mixtures were individually loaded on the Superdex 200 increase 10/300 GL column (GE Healthcare) in the same volume and superposed for UV absorption peaks. The eluted proteins were analyzed by SDS-PAGE.

2.10. Native-PAGE

The 10% native-PAGE gel and running buffer were prepared without SDS. The pAPN ectodomain and PEDV S1 or S1t protein were mixed in 30 μl 20 mM Tris-HCl pH 7.6, 150 mM NaCl at a molar ratio of 1:1/1:5. After incubation at RT for 30 min, PEDV S1 or S1t protein, pAPN ectodomain and their mixtures were analyzed by native-PAGE.

2.11. Surface plasmon resonance (SPR) analyses

SPR analyses were performed on Biacore S200 (GE Healthcare) to determine the equilibrium binding constants (K_D, M), the association rate constants (K_{on}, $M^{-1}\,S^{-1}$) and the dissociation rate constants (K_{off}, S^{-1}) of pAPN ectodomain binding to PEDV S1 or S1t protein. PEDV S1 or S1t protein was coupled to the CM5 sensor chips (GE Healthcare) and pAPN ectodomain was injected with the indicated concentrations (187.5 nM, 375 nM, 750 nM, 1500 nM and 3000 nM). The running buffer was HBS-EP (10 mM Hepes pH 7.4, 150 mM NaCl, 3 mM EDTA, 0.005% Surfactant P20). The binding kinetics were analyzed with the software Biacore S200 evaluation 1.0, and the K_{on}, K_{off} and K_D were calculated using a 1:1 interaction model as previously described [47]. The equations used for calculation are represented below with Biacore SPR terminology:

$$K_D = \frac{K_{off}}{K_{on}},$$

$$\frac{dR}{dt} = K_{on} \cdot C \cdot (Rmax - R) - K_{off} \cdot R,$$

where $\frac{dR}{dt}$ (response unit/s, RU/s) is the slope of the curve during association phase, C (M) is the concentration of injected pAPN ectodomain, Rmax (RU) is the signal response for maximum absorption of PEDV S1or S1t protein, and R (RU) is the signal response for pAPN ectodomain binding to PEDV S1 or S1t protein.

2.12. Statistical analysis

All experimental data were presented as group means and standard errors of the means (SEM). The experimental data were analyzed using the unpaired, 2-tailed Student *t*-test using GraphPad Prism software (GraphPad). Differences at the 95% confidence level ($p < 0.05$) were considered statistically significant.

3. Results and discussion

3.1. Expression of recombinant proteins

The recombinant pAPN ectodomain (residues 63–963), PEDV S1 protein (residues 21–793) and S1 truncated variants (residues 21–249, 253–638 and 505–629) were produced in *Drosophila* S2 cells. Western blot analyses verified that pAPN ectodomain (Fig. 1A), PEDV S1 protein (Fig. 1B) and a PEDV S1 truncated variant (S1t, residues 505–629, Fig. 1C) were highly expressed. The expression of other PEDV S1 truncated variants (residues 21–249 and 253–638) was too low to be detected (data not shown), which were consequently not considered in our subsequent experiments.

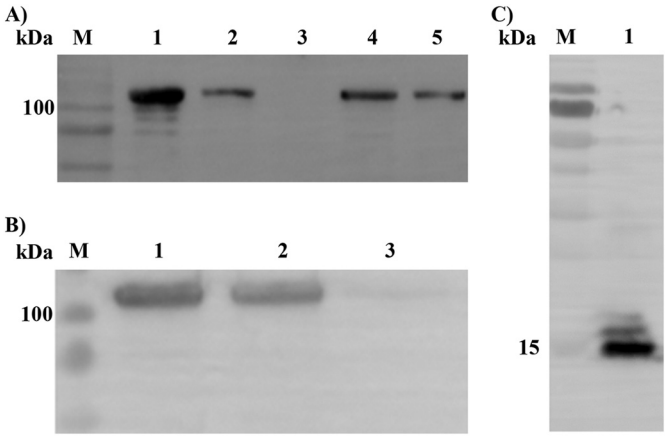

Fig. 1. Western blot analyses of the expression of recombinant proteins. (A): pAPN ectodomain (residues 63–963). Lane 1, 2, 4, 5: pAPN ectodomain; Lane 3: mock. (B): PEDV S1 protein (residues 21–793). Lane 1–2: PEDV S1 protein; Lane 3: mock. (C): PEDV S1 truncated variant (S1t, residues 505–629). Lane 1: PEDV S1t protein. Lane M: Thermo pre-stained protein ladder (10 to 180 kDa).

3.2. Purification of recombinant proteins

The target proteins were purified through metal-affinity and size-exclusion chromatography. After purification, these proteins achieved to a high purity (>99%, Fig. 2). pAPN ectodomain (Fig. 2, top), PEDV S1 (Fig. 2, middle) and S1t proteins (Fig. 2, bottom) were eluted at 10.9 ml, 12.2 ml and 17.8 ml on the calibrated size-exclusion column, corresponding to approximately 240 kDa, 110 kDa, 15 kDa, respectively. As shown in Fig. 2, there were differences between the bands of each target protein under reducing (Lane 2) and non-reducing (Lane 1) conditions, which implied that they contained disulfide bonds. In addition, the bands showed a significant change after de-glycosylation using PNGase F (Lane 2 and Lane 3). Therefore, the recombinant proteins were heavily glycosylated compared to their calculated molecular masses (pAPN ectodomain: 104 kDa, PEDV S1 protein: 85.5 kDa, PEDV S1t protein: 15.1 kDa). Based on the results above, recombinant pAPN ectodomain was obtained as dimers, and PEDV S1 or S1t protein existed as monomers, which showed similar natures of mammalian APN [43] and other coronavirus S proteins [48–50] as previously reported.

3.3. Immunogenicity tests, interference of PEDV binding and CD measurements of purified PEDV S1 and S1t proteins

We carried out immunogenicity tests and PEDV binding interference assays to analyze whether purified PEDV S1 and S1t proteins were functional. As shown in Fig. 3A and B, purified PEDV S1 and S1t proteins could be recognized by positive serum against PEDV, indicating that these recombinant proteins had a comparable immunogenicity to the native virus. Since porcine small intestines are the major target organ for PEDV infection, IPEC-J2 cells from porcine small intestines were applied in interference of PEDV binding by purified PEDV S1 and S1t proteins. IPEC-J2 cells incubated with PEDV S1 or S1t protein showed the viral RNA reduction in a concentration dependent manner (Fig. 3C). Especially at a concentration of 200 μg/mL, PEDV S1 or S1t protein pretreatment caused a significant reduction compared to that incubated with control protein buffer ($p < 0.05$), demonstrating that purified PEDV S1 and S1t proteins were in functional form (Fig. 3C).

We have taken efforts to crystallize functional PEDV S1 or S1t protein, and determine their crystal structures. Unfortunately, crystallization of these proteins was unsuccessful (data not shown). CD measurement is usual for determination of protein secondary structures

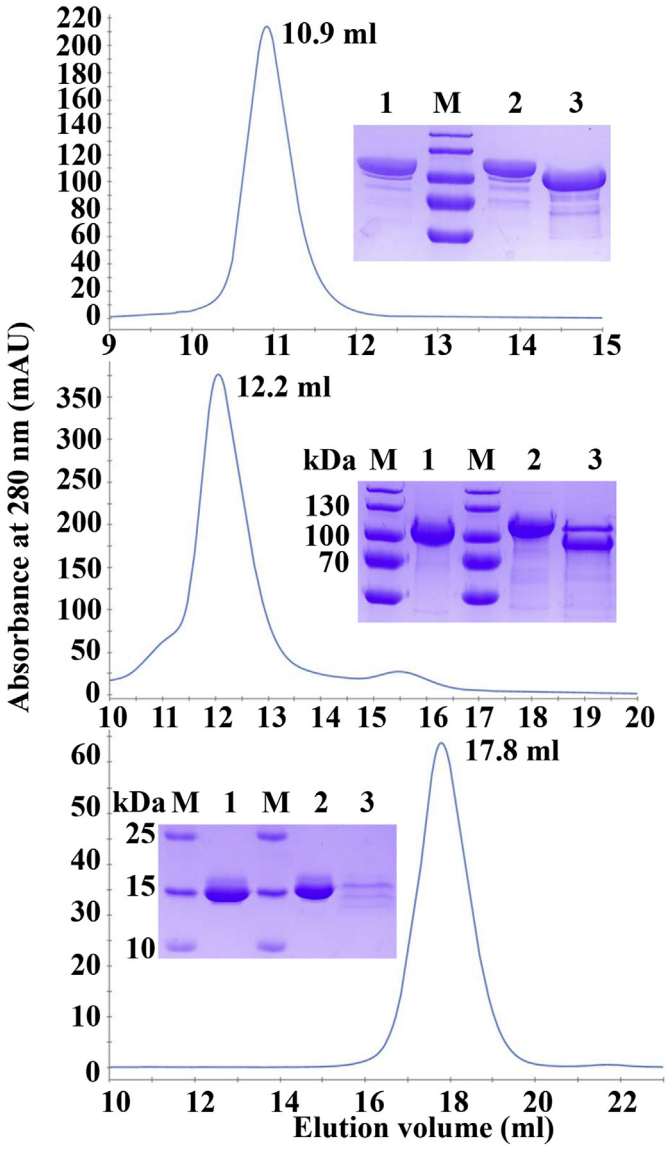

Fig. 2. Size-exclusion chromatography and SDS-PAGE analyses of recombinant pAPN ectodomain (top), PEDV S1 protein (middle) and PEDV S1t protein (bottom). Lane 1: The target protein under non-reducing condition without β-mercaptoethanol; Lane 2: The target protein under reducing condition with β-mercaptoethanol; Lane 3: The target protein treated with PNGase F under reducing condition. Lane M: Thermo pre-stained protein ladder (10 to 180 kDa).

[51–56] and we performed CD measurements to study their secondary structures. As shown in Fig. 4, one minimum at about 215 nm was observed for both PEDV S1 and S1t proteins, suggesting that the two proteins had β-sheets. These results were consistent with other coronavirus S1 proteins, which have a high content of β-sheets [49,50,57–60].

3.4. Functional and structural studies of purified pAPN ectodomain

Mammalian APN is a member of zinc-dependent M1 metallopeptidases, which is widely distributed on the intestinal epithelia and the nervous system cells [61]. It plays multifunctional roles in tumor angiogenesis and metastasis, signal pathway, and degradation of enkephalins [62]. Based on these functions, we performed activity assay for purified pAPN ectodomain. The enzymatic kinetics showed

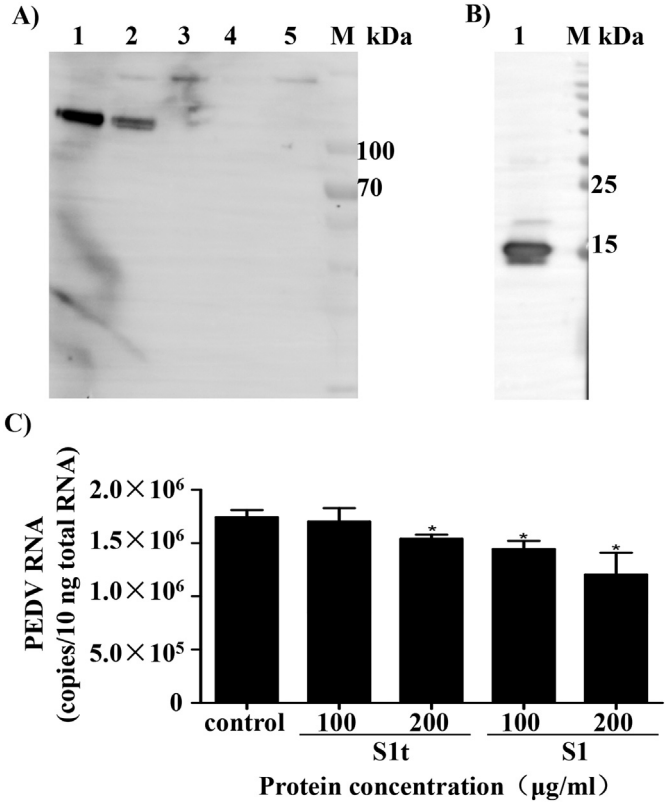

Fig. 3. Immunogenicity tests and interference of PEDV binding by purified S1 and S1t proteins. Purified PEDV S1 (A) and S1t proteins (B) were detected by Western blot using the positive antiserum against PEDV. (C) PEDV binding interference with purified PEDV S1 or S1t protein. Data represent means ± SEM of three independent experiments. *Significantly reduced viral RNA ($p < 0.05$).

that purified pAPN ectodomain could degrade the substrate L-alanine 4-nitroanilide hydrochloride into the product *p*-nitroanilide. The K_m and K_{cat} were 0.18 ± 0.13 mM and 75.55 ± 7.9/s, respectively (Table 2).

Furthermore, we determined the crystal structure of pAPN ectodomain. Purified pAPN ectodomain was crystallized with one molecule in each asymmetric unit and its crystal structure was determined at 2.65 Å in a C121 space group (Table 3). As described previously [22,24,43,63,64], pAPN ectodomain adopts a hook-like conformation or so-called seahorse shape (Fig. 5B and C). It is consisted of four domains (I-IV) and a zinc ion in Domain II, characteristics of M1 metallopeptidases (Fig. 5A and B). In addition, it is heavily glycosylated, and Cys758 and Cys765 in association with Cys795 and Cys831 bridge into two disulfide linkages in Domain IV (Fig. 5B), which are consistent with our results stated above (Fig. 2). A close structural comparison of our current pAPN ectodomain and that determined by others (PDB code: 4HOM) reveals that the root mean square deviation (RMSD) differences are slight (0.361 Å for 853 matching Cα atoms), demonstrating that they share almost identical structural fold (Fig. 5C).

Taken together, purified pAPN ectodomain was shown to be biologically active on the basis of its enzymatic activity and crystal structure.

Table 3
X-ray data collection and model refinement statistics.

Crystal	pAPN ectodomain
PDB code	5Z65
X-ray source wavelength (Å)	0.979
Resolution limits (Å)	2.65
Space group	C121
Temperature of experiments (K)	100
Cell parameters (Å)	a = 260.3, b = 62.3, c = 80.6, α = 90°, β = 100°, γ = 90°
Completeness (%)	99.6 (99.6)[a]
Redundancy	6.4 (6.3)[a]
Rmerge[b]	0.137 (1.287)[a]
Number of observations	236,643
Number of unique reflections	37,252
Refinement data	
R factor	0.196
R free	0.251
r.m.s deviation of bond lengths (Å^2)	0.019
r.m.s deviation of angle (°)	1.984
Ramachandran analysis (%)	95.0[c], 4.6[d], 0.4[e]

[a] Numbers in parentheses refer to the highest resolution shells.
[b] Rmerge = Σ|*Ii*−<*I*>|/Σ*Ii*, where *Ii* is the intensity of the h observation and <*I*> is the mean intensity of the reflections.
[c] Percentage of residues in most favored regions.
[d] Percentage of residues in additional allowed regions.
[e] Percentage of residues in generously allowed regions.

3.5. Characterization of the interaction between functional pAPN ectodomain and PEDV S proteins

pAPN was previously demonstrated as a functional receptor for PEDV [31–34]. However, the Vero cell lines, possessing no APN

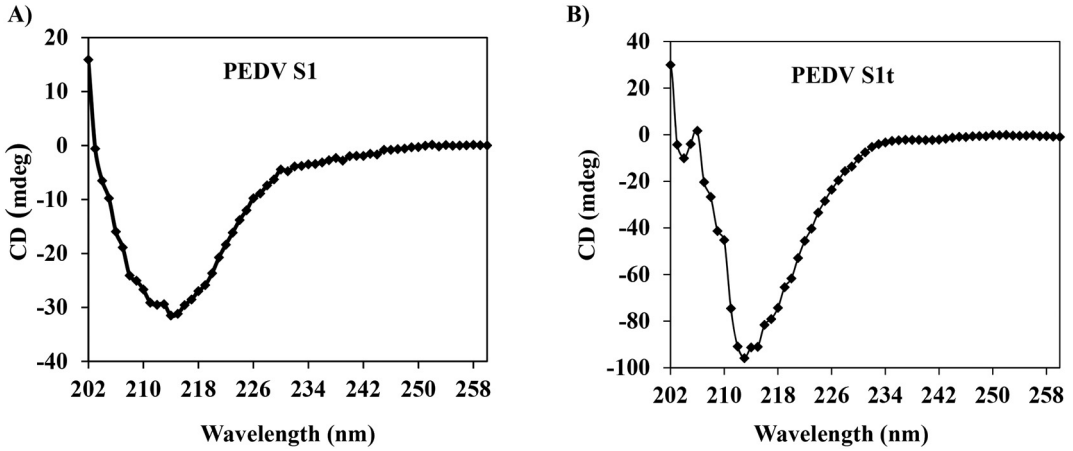

Fig. 4. CD spectra of functional PEDV S1 (A) and S1t proteins (B). One minimum at about 215 nm was observed for both PEDV S1 and S1t proteins.

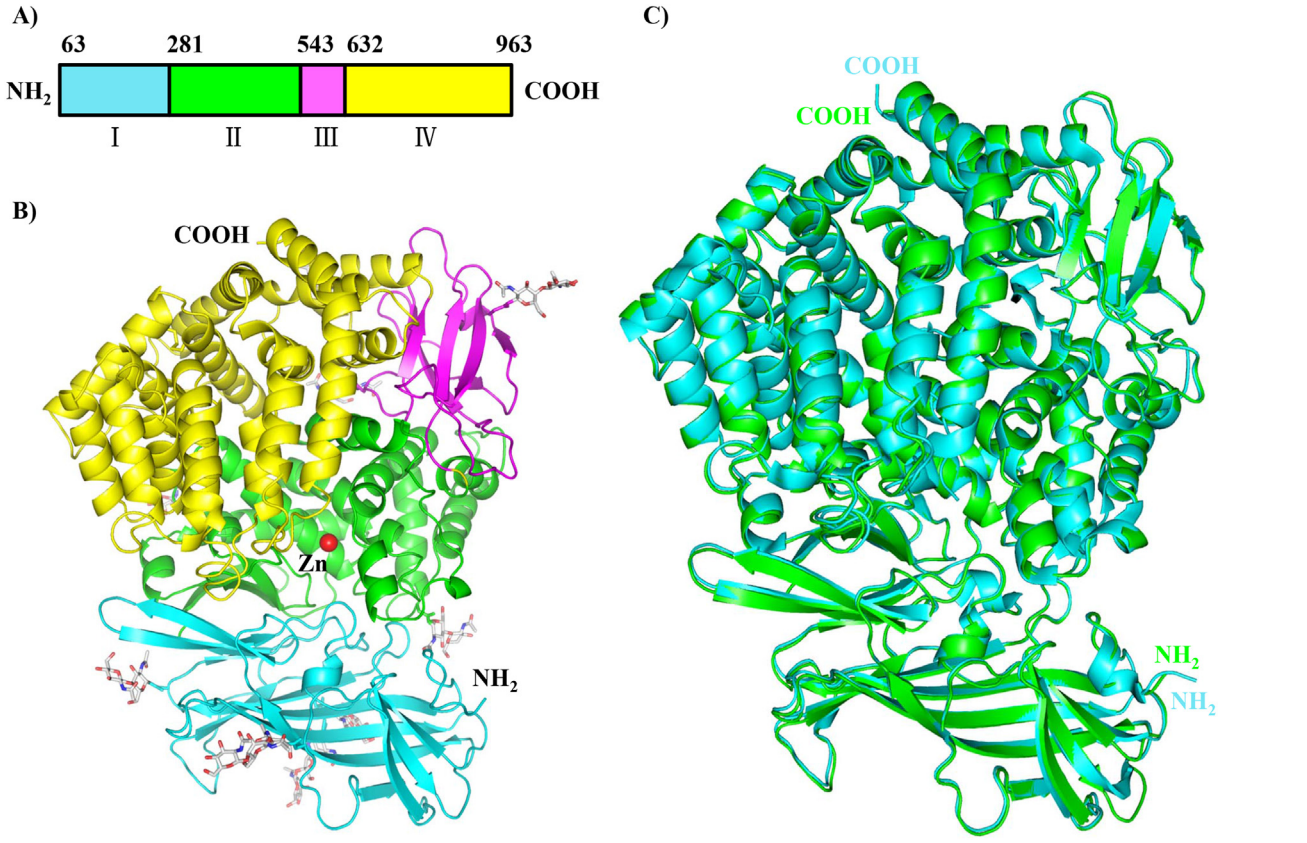

Fig. 5. Crystal structure of functional pAPN ectodomain. (A): Schematic diagram of pAPN ectodomain. pAPN ectodomain is consisted of four domains (I–IV). Domain I (residues 63–280) is in cyan, Domain II (residues 281–542) is in green, Domain III (residues 543–631) is in magenta, and Domain IV (residues 632–963) is in yellow. (B) Cartoon diagram of pAPN ectodomain. pAPN ectodomain is colored as described for (A). The zinc ion is represented as red sphere and N-linked oligosaccharides are shown in stick representation. The N and the C termini are also labeled. (C) Structural comparison of pAPN ectodomain in the current study with that determined by others (PDB code 4HOM) in cartoon diagrams. The pAPN ectodomain in the current study is colored in green and the pAPN ectodomain previously determined is in cyan. Their N and C termini are labeled.

[32,41], are efficiently infected by PEDV, and widely utilized for isolation and series propagation of the virus [41,65–68]. Recently, no effects were reported on the susceptibility to PEDV after knocking out APN in porcine swine testis cells and human cell lines (human hepatoma cells, Huh7 cells and human cervical cancer cells, HeLa cells) by CRISPR/Cas9 genome editing [38]. Moreover, soluble pAPN ectodomain neither interacted with PEDV nor inhibited its infection [37]. All these studies infer that pAPN may be not the receptor for PEDV. To date, there are few direct evidences to clarify this discrepancy by characterization of the interaction between pAPN ectodomain and PEDV S protein *in vitro*.

We speculate that the lack of related studies is probably due to the difficulty in preparing the large PEDV S protein, which contains many disulfide bonds and glycosylation sites as other coronaviruses [48,49]. In the current study, three canonical assays were carried out to characterize the interaction between pAPN ectodomain and PEDV S1 or S1t protein since these functional target proteins were successfully prepared. According to previous reports, coronavirus S-RBDs and their host receptors have high affinities and yield stable complexes *in vitro*, which can be obtained by gel filtration chromatography [17,20,22,24,69,70]. Therefore, we firstly characterized the interaction between pAPN ectodomain and PEDV S1 or S1t protein by gel filtration chromatography. The results showed that there were no complexes formed in these protein mixtures as no complex peaks appeared (Fig. 6). Additionally, we performed native-PAGE to detect whether they formed complexes. As shown in Fig. 7A, there were no bands of the protein complexes compared to single proteins. Interestingly, PEDV S1t protein showed other forms in addition to monomers (Figs. 6B and 7A). In order to further corroborate the interaction between the proteins, the kinetics of pAPN ectodomain binding to PEDV S1 or S1t protein were measured by SPR using Biacore S200. The profiles showed that there were no signal responses during their association and dissociation phases, which demonstrated that pAPN ectodomain neither interacted with PEDV S1 nor S1t protein under physiological condition (Fig. 7B). In contrast, HCoV-229E [22] and TGEV [24] RBDs had high affinities to their receptor APN. These results were similar to SARS-CoV RBD not binding to DPP4 or MERS-CoV RBD not binding to ACE2, while the K_D of DPP4 binding to MERS-CoV RBD was about 16.7 nM (K_{on}: 1.79×10^5 M^{-1} s^{-1}, K_{off}: 2.99×10^{-3} M^{-1} s^{-1}) [20].

In conclusion, our work characterized the interaction between recombinant pAPN ectodomain and PEDV S protein *in vitro*. The results suggest that pAPN may be controversial as the genuine receptor for PEDV because functional pAPN ectodomain neither binds to PEDV S1 nor S1t protein. Our current work sheds some light on the invasion mechanism of the virus, and supports a molecular basis for prevention and control of PED. As S protein recognizing and interacting with the host receptor are crucial for PEDV infection, further research needs to be carried out to identify the genuine receptor of PEDV and elucidate the specific interaction between them.

Disclosure of conflict of interest

The authors declare that they have no conflicts of interest.

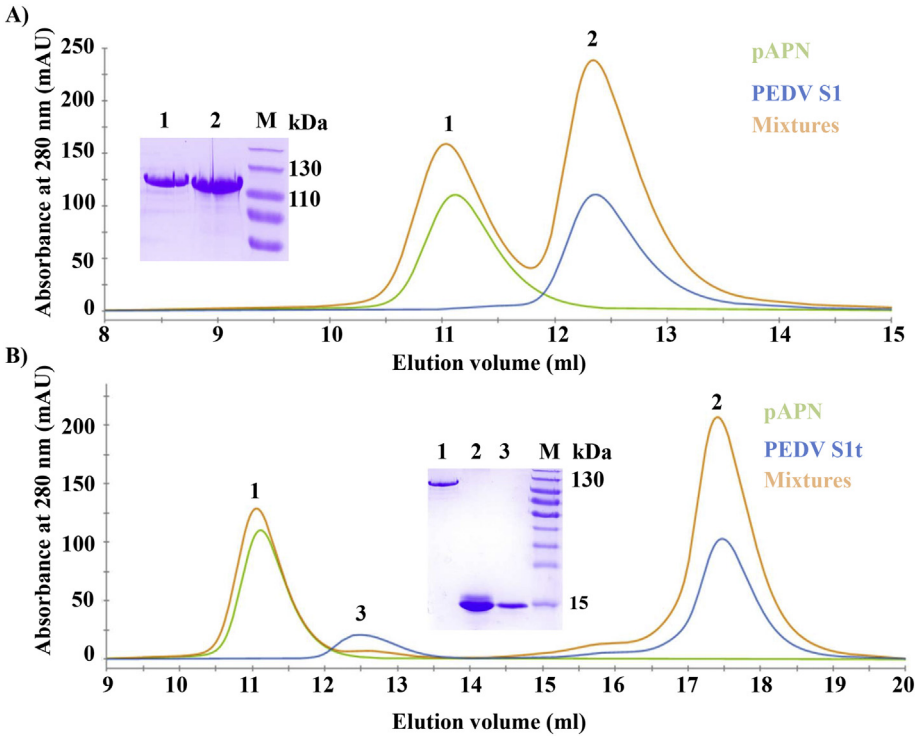

Fig. 6. Gel filtration chromatography analyses of PEDV S1 or S1t protein (blue), pAPN ectodomain (green) and their mixtures (brown). The pAPN ectodomain, PEDV S1 (A) or S1t protein (B) and their mixtures were loaded on a calibrated Superdex 200 increase column (10/300 GL) individually. Their chromatographs were superposed and shown in the figures. SDS-PAGE analyses of pooled samples (A: 1–2 and B: 1–3) were also presented.

Acknowledgements

We thank the staff of BL19U1 beamline at National Center for Protein Sciences Shanghai (NCPSS) and Shanghai Synchrotron Radiation Facility (SSRF), Shanghai, China, for assistance during data collection. We also acknowledge Qiang Wei and Hongfang Ma from Henan Academy of Agricultural Sciences for their assistance on crystallization, and Baolin Xiao from Henan University for his assistance on CD measurements. This work was supported by the Earmarked Fund for Modern Agro-industry Technology Research System of China (CARS-35), the Special Fund for Henan Agriculture Research System (S2012-06), the funds from the Natural Science Foundation of Henan Province (182300410001) and Henan Academy of Agricultural Sciences ([2017]76-22 and 20188118). The

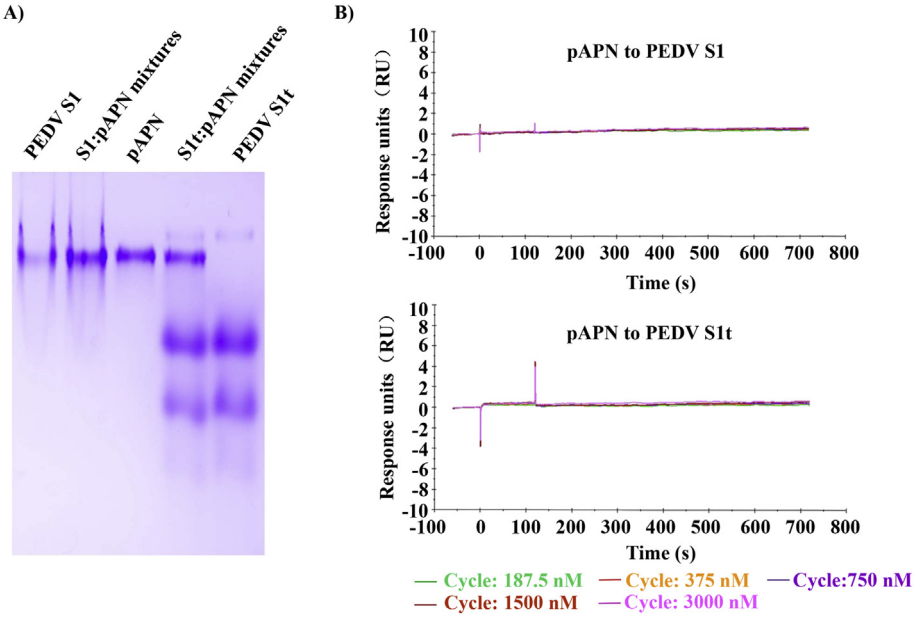

Fig. 7. Characterization of the interaction between pAPN ectodomain and PEDV S1 or S1t protein. (A): Native-PAGE analysis. Lane 1: PEDV S1 protein; Lane 2: pAPN ectodomain and PEDV S1 protein mixtures (1:1); Lane 3: pAPN ectodomain; Lane 4: pAPN ectodomain and PEDV S1t protein mixtures (1:5); Lane 5: PEDV S1t protein. (B): SPR analyses of the interaction between PEDV S1 (top) or S1t protein (bottom) and pAPN ectodomain.

funders had no role in study design, data collection and interpretation, or the decision to submit the work for publication.

References

[1] P.C. Woo, Y. Huang, S.K. Lau, K.Y. Yuen, Coronavirus genomics and bioinformatics analysis, Viruses 2 (8) (2010) 1804–1820.

[2] T.G. Ksiazek, D. Erdman, C.S. Goldsmith, S.R. Zaki, T. Peret, S. Emery, S. Tong, C. Urbani, J.A. Comer, W. Lim, P.E. Rollin, S.F. Dowell, A.E. Ling, C.D. Humphrey, W.J. Shieh, J. Guarner, C.D. Paddock, P. Rota, B. Fields, J. DeRisi, J.Y. Yang, N. Cox, J.M. Hughes, J.W. LeDuc, W.J. Bellini, L.J. Anderson, S.W. Group, A novel coronavirus associated with severe acute respiratory syndrome, N. Engl. J. Med. 348 (20) (2003) 1953–1966.

[3] T. Gallagher, S. Perlman, Public health: broad reception for coronavirus, Nature 495 (7440) (2013) 176–177.

[4] J.S. Peiris, S.T. Lai, L.L. Poon, Y. Guan, L.Y. Yam, W. Lim, J. Nicholls, W.K. Yee, W.W. Yan, M.T. Cheung, V.C. Cheng, K.H. Chan, D.N. Tsang, R.W. Yung, T.K. Ng, K.Y. Yuen, S.S. Group, Coronavirus as a possible cause of severe acute respiratory syndrome, Lancet 361 (9366) (2003) 1319–1325.

[5] M.A. Marra, S.J. Jones, C.R. Astell, R.A. Holt, A. Brooks-Wilson, Y.S. Butterfield, J. Khattra, J.K. Asano, S.A. Barber, S.Y. Chan, A. Cloutier, S.M. Coughlin, D. Freeman, N. Girn, O.L. Griffith, S.R. Leach, M. Mayo, H. McDonald, S.B. Montgomery, P.K. Pandoh, A.S. Petrescu, A.G. Robertson, J.E. Schein, A. Siddiqui, D.E. Smailus, J.M. Stott, G.S. Yang, F. Plummer, A. Andonov, H. Artsob, N. Bastien, K. Bernard, T.F. Booth, D. Bowness, M. Czub, M. Drebot, L. Fernando, R. Flick, M. Garbutt, M. Gray, A. Grolla, S. Jones, H. Feldmann, A. Meyers, A. Kabani, Y. Li, S. Normand, U. Stroher, G.A. Tipples, S. Tyler, R. Vogrig, D. Ward, B. Watson, R.C. Brunham, M. Krajden, M. Petric, D.M. Skowronski, C. Upton, R.L. Roper, The Genome sequence of the SARS-associated coronavirus, Science 300 (5624) (2003) 1399–1404.

[6] P.A. Rota, M.S. Oberste, S.S. Monroe, W.A. Nix, R. Campagnoli, J.P. Icenogle, S. Penaranda, B. Bankamp, K. Maher, M.H. Chen, S. Tong, A. Tamin, L. Lowe, M. Frace, J.L. DeRisi, Q. Chen, D. Wang, D.D. Erdman, T.C. Peret, C. Burns, T.G. Ksiazek, P.E. Rollin, A. Sanchez, S. Liffick, B. Holloway, J. Limor, K. McCaustland, M. Olsen-Rasmussen, R. Fouchier, S. Gunther, A.D. Osterhaus, C. Drosten, M.A. Pallansch, L.J. Anderson, W.J. Bellini, Characterization of a novel coronavirus associated with severe acute respiratory syndrome, Science 300 (5624) (2003) 1394–1399.

[7] A. Bermingham, M.A. Chand, C.S. Brown, E. Aarons, C. Tong, C. Langrish, K. Hoschler, K. Brown, M. Galiano, R. Myers, R.G. Pebody, H.K. Green, N.L. Boddington, R. Gopal, N. Price, W. Newsholme, C. Drosten, R.A. Fouchier, M. Zambon, Severe respiratory illness caused by a novel coronavirus, in a patient transferred to the United Kingdom from the Middle East, September 2012, Euro Surveill. 17 (40) (2012) 20290.

[8] A.M. Zaki, S. van Boheemen, T.M. Bestebroer, A.D. Osterhaus, R.A. Fouchier, Isolation of a novel coronavirus from a man with pneumonia in Saudi Arabia, N. Engl. J. Med. 367 (19) (2012) 1814–1820.

[9] R.J. de Groot, S.C. Baker, R.S. Baric, C.S. Brown, C. Drosten, L. Enjuanes, R.A. Fouchier, M. Galiano, A.E. Gorbalenya, Z.A. Memish, S. Perlman, L.L. Poon, E.J. Snijder, G.M. Stephens, P.C. Woo, A.M. Zaki, M. Zambon, J. Ziebuhr, Middle East respiratory syndrome coronavirus (MERS-CoV): announcement of the Coronavirus Study Group, J. Virol. 87 (14) (2013) 7790–7792.

[10] B. Guery, J. Poissy, L. el Mansouf, C. Sejourne, N. Ettahar, X. Lemaire, F. Vuotto, A. Goffard, S. Behillil, V. Enouf, V. Caro, A. Mailles, D. Che, J.C. Manuguerra, D. Mathieu, A. Fontanet, S. van der Werf, M.E.-C.s. Group, Clinical features and viral diagnosis of two cases of infection with Middle East Respiratory Syndrome coronavirus: a report of nosocomial transmission, Lancet 381 (9885) (2013) 2265–2272.

[11] L. Enjuanes, C. Smerdou, C.M. Sanchez, C. Sune, S. Kelly, R. Curtiss 3rd, J.M. Torres, Induction of transmissible gastroenteritis coronavirus specific immune responses using vectors with enteric tropism, Adv. Exp. Med. Biol. 371B (1995) 1535–1541.

[12] J.K. Millet, G.R. Whittaker, Host cell proteases: critical determinants of coronavirus tropism and pathogenesis, Virus Res. 202 (2015) 120–134.

[13] S. Belouzard, J.K. Millet, B.N. Licitra, G.R. Whittaker, Mechanisms of coronavirus cell entry mediated by the viral spike protein, Viruses 4 (6) (2012) 1011–1033.

[14] F. Li, Receptor recognition mechanisms of coronaviruses: a decade of structural studies, J. Virol. 89 (4) (2015) 1954–1964.

[15] F. Li, Structure, function, and evolution of coronavirus spike proteins, Ann. Rev. Virol. 3 (1) (2016) 237–261.

[16] W. Li, M.J. Moore, N. Vasilieva, J. Sui, S.K. Wong, M.A. Berne, M. Somasundaran, J.L. Sullivan, K. Luzuriaga, T.C. Greenough, H. Choe, M. Farzan, Angiotensin-converting enzyme 2 is a functional receptor for the SARS coronavirus, Nature 426 (6965) (2003) 450–454.

[17] F. Li, W. Li, M. Farzan, S.C. Harrison, Structure of SARS coronavirus spike receptor-binding domain complexed with receptor, Science 309 (5742) (2005) 1864–1868.

[18] V.S. Raj, H. Mou, S.L. Smits, D.H. Dekkers, M.A. Muller, R. Dijkman, D. Muth, J.A. Demmers, A. Zaki, R.A. Fouchier, V. Thiel, C. Drosten, P.J. Rottier, A.D. Osterhaus, B.J. Bosch, B.L. Haagmans, Dipeptidyl peptidase 4 is a functional receptor for the emerging human coronavirus-EMC, Nature 495 (7440) (2013) 251–254.

[19] N. Wang, X. Shi, L. Jiang, S. Zhang, D. Wang, P. Tong, D. Guo, L. Fu, Y. Cui, X. Liu, K.C. Arledge, Y.H. Chen, L. Zhang, X. Wang, Structure of MERS-CoV spike receptor-binding domain complexed with human receptor DPP4, Cell Res. 23 (8) (2013) 986–993.

[20] G. Lu, Y. Hu, Q. Wang, J. Qi, F. Gao, Y. Li, Y. Zhang, W. Zhang, Y. Yuan, J. Bao, B. Zhang, Y. Shi, J. Yan, G.F. Gao, Molecular basis of binding between novel human coronavirus MERS-CoV and its receptor CD26, Nature 500 (7461) (2013) 227–231.

[21] C.L. Yeager, R.A. Ashmun, R.K. Williams, C.B. Cardellichio, L.H. Shapiro, A.T. Look, K.V. Holmes, Human aminopeptidase N is a receptor for human coronavirus 229E, Nature 357 (6377) (1992) 420–422.

[22] A.H.M. Wong, A.C.A. Tomlinson, D. Zhou, M. Satkunarajah, K. Chen, C. Sharon, M. Desforges, P.J. Talbot, J.M. Rini, Receptor-binding loops in alphacoronavirus adaptation and evolution, Nat. Commun. 8 (1) (2017) 1735.

[23] B. Delmas, J. Gelfi, R. L'Haridon, L.K. Vogel, H. Sjostrom, O. Noren, H. Laude, Aminopeptidase N is a major receptor for the entero-pathogenic coronavirus TGEV, Nature 357 (6377) (1992) 417–420.

[24] J. Reguera, C. Santiago, G. Mudgal, D. Ordono, L. Enjuanes, J.M. Casasnovas, Structural bases of coronavirus attachment to host aminopeptidase N and its inhibition by neutralizing antibodies, PLoS Pathog. 8 (8) (2012), e1002859.

[25] R. Li, S. Qiao, Y. Yang, Y. Su, P. Zhao, E. Zhou, G. Zhang, Phylogenetic analysis of porcine epidemic diarrhea virus (PEDV) field strains in central China based on the ORF3 gene and the main neutralization epitopes, Arch. Virol. 159 (5) (2014) 1057–1065.

[26] J. Bi, S. Zeng, S. Xiao, H. Chen, L. Fang, Complete genome sequence of porcine epidemic diarrhea virus strain AJ1102 isolated from a suckling piglet with acute diarrhea in China, J. Virol. 86 (19) (2012) 10910–10911.

[27] Y. Tian, Z. Yu, K. Cheng, Y. Liu, J. Huang, Y. Xin, Y. Li, S. Fan, T. Wang, G. Huang, N. Feng, Z. Yang, S. Yang, Y. Gao, X. Xia, Molecular characterization and phylogenetic analysis of new variants of the porcine epidemic diarrhea virus in Gansu, China in 2012, Viruses 5 (8) (2013) 1991–2004.

[28] G. Cima, Viral disease affects U.S. pigs: porcine epidemic diarrhea found in at least 11 states, J. Am. Vet. Med. Assoc. 243 (1) (2013) 30–31.

[29] A.N. Vlasova, D. Marthaler, Q. Wang, M.R. Culhane, K.D. Rossow, A. Rovira, J. Collins, L.J. Saif, Distinct characteristics and complex evolution of PEDV strains, North America, May 2013–February 2014, Emerg. Infect. Dis. 20 (10) (2014) 1620–1628.

[30] S. Park, S. Kim, D. Song, B. Park, Novel porcine epidemic diarrhea virus variant with large genomic deletion, South Korea, Emerg. Infect. Dis. 20 (12) (2014) 2089–2092.

[31] J.S. Oh, D.S. Song, B.K. Park, Identification of a putative cellular receptor 150 kDa polypeptide for porcine epidemic diarrhea virus in porcine enterocytes, J. Vet. Sci. 4 (3) (2003) 269–275.

[32] B.X. Li, J.W. Ge, Y.J. Li, Porcine aminopeptidase N is a functional receptor for the PEDV coronavirus, Virology 365 (1) (2007) 166–172.

[33] C. Liu, J. Tang, Y. Ma, X. Liang, Y. Yang, G. Peng, Q. Qi, S. Jiang, J. Li, L. Du, F. Li, Receptor usage and cell entry of porcine epidemic diarrhea coronavirus, J. Virol. 89 (11) (2015) 6121–6125.

[34] J.E. Park, E.S. Park, J.E. Yu, J. Rho, S. Paudel, B.H. Hyun, D.K. Yang, H.J. Shin, Development of transgenic mouse model expressing porcine aminopeptidase N and its susceptibility to porcine epidemic diarrhea virus, Virus Res. 197 (2015) 108–15.

[35] E. Nam, C. Lee, Contribution of the porcine aminopeptidase N (CD13) receptor density to porcine epidemic diarrhea virus infection, Vet. Microbiol. 144 (1–2) (2010) 41–50.

[36] F. Deng, G. Ye, Q. Liu, M.T. Navid, X. Zhong, Y. Li, C. Wan, S. Xiao, Q. He, Z.F. Fu, G. Peng, Identification and comparison of receptor binding characteristics of the spike protein of two porcine epidemic diarrhea virus strains, Viruses 8 (3) (2016) 55.

[37] K. Shirato, M. Maejima, M.T. Islam, A. Miyazaki, M. Kawase, S. Matsuyama, F. Taguchi, Porcine aminopeptidase N is not a cellular receptor of porcine epidemic diarrhea virus, but promotes its infectivity via aminopeptidase activity, J. Gen. Virol. 97 (10) (2016) 2528–2539.

[38] W. Li, R. Luo, Q. He, F.J.M. van Kuppeveld, P.J.M. Rottier, B.J. Bosch, Aminopeptidase N is not required for porcine epidemic diarrhea virus cell entry, Virus Res. 235 (2017) 6–13.

[39] H. Ma, L. Jiang, S. Qiao, Y. Zhi, X.X. Chen, Y. Yang, X. Huang, M. Huang, R. Li, G.P. Zhang, The crystal structure of the fifth scavenger receptor cysteine-rich domain of porcine CD163 reveals an important residue involved in porcine reproductive and respiratory syndrome virus infection, J. Virol. 91 (3) (2017).

[40] R. Li, H. Ma, L. Jiang, S. Qiao, Y. Zhi, M. Huang, R. Deng, G. Zhang, The CD163 long-range scavenger receptor cysteine-rich repeat: expression, purification and X-ray crystallographic characterization, Acta Crystallogr. F Struct. Biol. Commun. 74 (Pt 5) (2018) 322–326.

[41] M. Hofmann, R. Wyler, Propagation of the virus of porcine epidemic diarrhea in cell culture, J. Clin. Microbiol. 26 (11) (1988) 2235–2239.

[42] Y. Su, Y. Liu, Y. Chen, G. Xing, H. Hao, Q. Wei, Y. Liang, W. Xie, D. Li, H. Huang, R. Deng, G. Zhang, A novel duplex TaqMan probe-based real-time RT-qPCR for detecting and differentiating classical and variant porcine epidemic diarrhea viruses, Mol. Cell. Probes 37 (2018) 6–11.

[43] L. Chen, Y.L. Lin, G. Peng, F. Li, Structural basis for multifunctional roles of mammalian aminopeptidase N, Proc. Natl. Acad. Sci. U. S. A. 109 (44) (2012) 17966–17971.

[44] N. Collaborative Computational Project, The CCP4 suite: programs for protein crystallography, Acta Crystallogr. D Biol. Crystallogr. 50 (Pt 5) (1994) 760–763.

[45] P. Emsley, K. Cowtan, Coot: model-building tools for molecular graphics, Acta Crystallogr. D Biol. Crystallogr. 60 (Pt 12 Pt 1) (2004) 2126–2132.

[46] W.L. DeLano, The PyMOL molecular graphics system, http://pymol.org 2002.

[47] J. Majka, C. Speck, Analysis of protein-DNA interactions using surface plasmon resonance, Adv. Biochem. Eng. Biotechnol. 104 (2007) 13–36.

[48] G. Ritchie, D.J. Harvey, F. Feldmann, U. Stroeher, H. Feldmann, L. Royle, R.A. Dwek, P.M. Rudd, Identification of N-linked carbohydrates from severe acute respiratory syndrome (SARS) spike glycoprotein, Virology 399 (2) (2010) 257–269.

[49] A.C. Walls, M.A. Tortorici, B. Frenz, J. Snijder, W. Li, F.A. Rey, F. DiMaio, B.J. Bosch, D. Veesler, Glycan shield and epitope masking of a coronavirus spike protein observed by cryo-electron microscopy, Nat. Struct. Mol. Biol. 23 (10) (2016) 899–905.

[50] X. Xiong, M.A. Tortorici, J. Snijder, C. Yoshioka, A.C. Walls, W. Li, A.T. McGuire, F.A. Rey, B.J. Bosch, D. Veesler, Glycan shield and fusion activation of a deltacoronavirus spike glycoprotein fine-tuned for enteric infections, J. Virol. 92 (4) (2017), e01628-17.

[51] P. Alam, G. Rabbani, G. Badr, B.M. Badr, R.H. Khan, The surfactant-induced conformational and activity alterations in *Rhizopus niveus* lipase, Cell Biochem. Biophys. 71 (2) (2015) 1199–1206.

[52] P. Alam, A.S. Abdelhameed, R.K. Rajpoot, R.H. Khan, Interplay of multiple interaction forces: binding of tyrosine kinase inhibitor nintedanib with human serum albumin, J. Photochem. Photobiol. B 157 (2016) 70–76.
[53] K. Laskar, P. Alam, R.H. Khan, A. Rauf, Synthesis, characterization and interaction studies of 1,3,4-oxadiazole derivatives of fatty acid with human serum albumin (HSA): a combined multi-spectroscopic and molecular docking study, Eur. J. Med. Chem. 122 (2016) 72–78.
[54] M.M. Alam, F. Abul Qais, I. Ahmad, P. Alam, R. Hasan Khan, I. Naseem, Multi-spectroscopic and molecular modelling approach to investigate the interaction of riboflavin with human serum albumin, J. Biomol. Struct. Dyn. 36 (3) (2018) 795–809.
[55] A.S. Abdelhameed, P. Alam, R.H. Khan, Binding of Janus kinase inhibitor tofacitinib with human serum albumin: multi-technique approach, J. Biomol. Struct. Dyn. 34 (9) (2016) 2037–2044.
[56] P. Alam, S.K. Chaturvedi, T. Anwar, M.K. Siddiqi, M.R. Ajmal, G. Badr, M.H. Mahmoud, R.H. Khan, Biophysical and molecular docking insight into the interaction of cytosine β-D arabinofuranoside with human serum albumin, J. Lumin. 164 (12) (2015) 123–130.
[57] A.C. Walls, M.A. Tortorici, B.J. Bosch, B. Frenz, P.J.M. Rottier, F. DiMaio, F.A. Rey, D. Veesler, Cryo-electron microscopy structure of a coronavirus spike glycoprotein trimer, Nature 531 (7592) (2016) 114–117.
[58] Y. Yuan, D. Cao, Y. Zhang, J. Ma, J. Qi, Q. Wang, G. Lu, Y. Wu, J. Yan, Y. Shi, X. Zhang, G.F. Gao, Cryo-EM structures of MERS-CoV and SARS-CoV spike glycoproteins reveal the dynamic receptor binding domains, Nat. Commun. 8 (2017), 15092.
[59] M. Gui, W. Song, H. Zhou, J. Xu, S. Chen, Y. Xiang, X. Wang, Cryo-electron microscopy structures of the SARS-CoV spike glycoprotein reveal a prerequisite conformational state for receptor binding, Cell Res. 27 (1) (2017) 119–129.
[60] J. Shang, Y. Zheng, Y. Yang, C. Liu, Q. Geng, W. Tai, L. Du, Y. Zhou, W. Zhang, F. Li, Cryo-EM structure of porcine delta coronavirus spike protein in the pre-fusion state, J. Virol. 94 (4) (2017), e01556-17.
[61] P. Mina-Osorio, The moonlighting enzyme CD13: old and new functions to target, Trends Mol. Med. 14 (8) (2008) 361–371.
[62] Y. Luan, W. Xu, The structure and main functions of aminopeptidase N, Curr. Med. Chem. 14 (6) (2007) 639–647.
[63] A.H. Wong, D. Zhou, J.M. Rini, The X-ray crystal structure of human aminopeptidase N reveals a novel dimer and the basis for peptide processing, J. Biol. Chem. 287 (44) (2012) 36804–36813.
[64] C. Santiago, G. Mudgal, J. Reguera, R. Recacha, S. Albrecht, L. Enjuanes, J.M. Casasnovas, Allosteric inhibition of aminopeptidase N functions related to tumor growth and virus infection, Sci. Rep. 7 (2017), 46045.
[65] K. Kusanagi, H. Kuwahara, T. Katoh, T. Nunoya, Y. Ishikawa, T. Samejima, M. Tajima, Isolation and serial propagation of porcine epidemic diarrhea virus in cell cultures and partial characterization of the isolate, J. Vet. Med. Sci. 54 (2) (1992) 313–318.
[66] T. Oka, L.J. Saif, D. Marthaler, M.A. Esseili, T. Meulia, C.M. Lin, A.N. Vlasova, K. Jung, Y. Zhang, Q. Wang, Cell culture isolation and sequence analysis of genetically diverse US porcine epidemic diarrhea virus strains including a novel strain with a large deletion in the spike gene, Vet. Microbiol. 173 (3–4) (2014) 258–269.
[67] S. Lee, Y. Kim, C. Lee, Isolation and characterization of a Korean porcine epidemic diarrhea virus strain KNU-141112, Virus Res. 208 (2015) 215–224.
[68] Y. Wang, X. Gao, Y. Yao, Y. Zhang, C. Lv, Z. Sun, Y. Wang, X. Jia, J. Zhuang, Y. Xiao, X. Li, K. Tian, The dynamics of Chinese variant porcine epidemic diarrhea virus production in Vero cells and intestines of 2-day old piglets, Virus Res. 208 (2015) 82–88.
[69] K. Wu, W. Li, G. Peng, F. Li, Crystal structure of NL63 respiratory coronavirus receptor-binding domain complexed with its human receptor, Proc. Natl. Acad. Sci. U. S. A. 106 (47) (2009) 19970–19974.
[70] G. Peng, D. Sun, K.R. Rajashankar, Z. Qian, K.V. Holmes, F. Li, Crystal structure of mouse coronavirus receptor-binding domain complexed with its murine receptor, Proc. Natl. Acad. Sci. U. S. A. 108 (26) (2011) 10696–10701.